Laser and Particle Beams (2004), *22*, 315–321. Printed in the USA.

DOI: 10.1017/S0263034604223163

Hot electron diagnostics using X-rays and Čerenkov radiation

J. STEIN,[1,2] E. FILL,[1] D. HABS,[2] G. PRETZLER,[3] AND K. WITTE[1]

[1]Max-Planck-Institut für Quantenoptik, Garching, Germany
[2]Ludwig-Maximilians-Universität München, Garching, Germany
[3]Universität Düsseldorf, Düsseldorf, Germany

(RECEIVED 1 November 2003; ACCEPTED 18 December 2003)

Abstract

The propagation of laser-generated hot electrons through matter and across narrow vacuum gaps is studied. We use the ATLAS titanium–sapphire laser of Max-Planck-Institut für Quantenoptik to irradiate aluminum and copper foils at intensities of up to 10^{19} W/cm^2, generating electrons with temperatures in the megaelectron volt range. After propagating through the target the electrons are detected by means of visible Čerenkov radiation generated in a dielectric or hard X-rays emitted from an X-ray "fluor." These diagnostics allow the electrons to be characterized with respect to their energy, number, and directionality. We also investigate the propagation of the hot electrons across narrow vacuum gaps, with a width ranging from 500 μm down to 50 μm. The effect of self-generated fields in preventing electrons from crossing the gap is demonstrated. Implications of these experiments with respect to fast ignitor physics, developing optics for fourth-generation light sources and X-ray lasers are indicated.

Keywords: Čerenkov radiation; Hot electrons; Laser plasmas; X-rays

1. INTRODUCTION

It is well known that the interaction of an intense laser pulse with a solid target generates hot electrons (Forslund *et al*., 1977; Gibbon and Förster, 1996; Borghesi *et al*., 1999; Davies *et al*., 1999; Gremillet *et al*., 1999; Eder *et al*., 2000; Batani *et al*., 2001; Feurer *et al*., 2001). These particles propagate further into the material and can be observed to emerge on the other side of the target. The great interest in this effect stems from applications of these electron beams in a variety of experiments and proposals, such as the hot igniter (Tabak *et al*., 1994), generation of high-energy protons and ions (Snavely *et al*., 2000; Wilks *et al*., 2001; Hegelich *et al*., 2002), ultrashort X-ray pulses, and X-ray lasers (Rose-Petruck *et al*., 1999; Fill, 2001*b*).

It is very important to characterize the generated electrons with respect to their abundance, energy, and directionality. The latter properties are a function of the mechanism of their generation. Electron diagnostics have relied on the generated X-rays (Wilks *et al*., 1992; Eder *et al*., 2000; Pretzler *et al*., 2000, 2001), backlighting with a visible pulse (Borghesi *et al*., 1999; Batani *et al*., 2001), and transition radiation (Santos *et al*., 2002). More recently a new method has been used to investigate features of the generated electron beams, namely, recording the visible Čerenkov radiation of the electrons emerging from the rear of the target in a suitable medium (Brandl *et al*., 2003). In this way the spatial features of the generated electrons can be determined as well as their numbers.

In this article we demonstrate the application of the Čerenkov method to investigate propagation of the electrons through foils. We further study the propagation of hot electrons across narrow vacuum gaps behind the primary target by means of X-ray diagnostics.

Čerenkov radiation is generated by particles exceeding the velocity of light in a dielectric. The Čerenkov detector widely used in high-energy physics is based on this effect. The classical theory of Čerenkov radiation (laid down by Frank and Tamm already in 1937, see Jelley, 1958) shows that the radiation is emitted in a cone of apex half-angle

$$\phi = \arccos(1/\beta n), \tag{1}$$

where β is the particle velocity divided by the vacuum light velocity and n is the refractive index of the medium. The intensity of the radiation per electron is given by the equation

Address correspondence and reprint requests to: Dr. Ernst Fill, Max-Planck-Institut für Quantenoptik, Hans-Kopfermann-Str. 1, D-85748 Garching, Germany. E-mail: ernst.fill@mpq.mpg.de

$$\frac{dW}{dl} = e^2/c^2 \int_{\beta n>1} [1 - 1/(\beta n)^2]\omega \, d\omega, \quad (2)$$

where l is the length along the path of the electron, e the elementary charge, and ω the frequency of the radiation. If the medium is thin enough to keep β unaltered along the particle path, the emission is proportional to the length of the medium. This is in contrast to optical transition radiation, which is generated only at the boundary of a medium. Radiation is emitted only in the visible and near UV regions of the spectrum, where $n > 1$ and where there is only little absorption. For a medium thin enough for β to be constant the number of photons emitted per electron at a wavelength λ in the interval $\Delta\lambda$ as derived from Eq. (2) is given by

$$N = 2\pi\alpha l \Delta\lambda/\lambda^2 [1 - 1/(\beta n)^2], \quad (3)$$

where $\alpha = 1/137$ is the fine-structure constant.

Equation (3) shows that Čerenkov radiation is quite an efficient process that may result in many photons per electron. The spectrum emitted sharply rises towards the UV region until anomalous dispersion and absorption eliminate the possibility of Čerenkov emission.

In the experiments reported in this article Čerenkov radiation is used to determine spatial features of the generated electron pulses. From these the mechanisms generating the electrons can be deduced. Furthermore, the radiation can be used to determine the number of generated electrons. Note that Čerenkov diagnostics probes only a certain window in the electron energy distribution, the lower end of which is determined by $\beta_{\min} = 1/n$ (emission on axis, see Eq. (1)). The upper limit of the electron energy detected is related to the *f*-number of the optics used for collecting the radiation. For electrons propagating on axis and symmetric imaging of the Čerenkov radiation it is given by

$$\beta_{\max} = 1/[n^2 - \sin^2(1/2f\#)]^{1/2}, \quad (4)$$

where *f*# is the *f*-number of the optics. For $n = 1.48$ and $f\# = 2$ one has a relatively small range of $\beta_{\min} = 0.67$ and $\beta_{\max} = 0.68$, corresponding to electron energies of 182 and 190 keV, respectively. However, if an angular spread of the electrons is taken into account, $\beta_{\min}$ is still given by $1/n$, but for $\beta_{\max}$ one obtains the expression

$$\beta_{\max} = \frac{1}{\cos\varphi[n^2 - \sin^2(1/2f\#)]^{1/2} - \sin\varphi \sin(1/2f\#)}. \quad (5)$$

Here φ is half the angular spread of the electron beam propagating in the Čerenkov medium. As an example, at an intensity of 5×10^{18} W/cm^2 the half angle of emission has been determined to be 12.5° (Brandl *et al.*, 2003) resulting in $\beta_{\max} = 0.73$ and a maximum energy of 236 keV.

A further interesting task of electron diagnostics is investigation of the effect of narrow vacuum gaps on the propagation of the electrons. In this case self-generated fields stop most of the electrons and prevent them from reaching a medium behind the gap. We demonstrate the effect of vacuum gaps by X-rays generated in a suitable "fluor" behind the target. The X-ray data are in good agreement with a simple theory treating self-fields of the electrons.

2. EXPERIMENTAL ARRANGEMENT

The experimental setup used is shown in Figure 1. Titanium–sapphire laser pulses from the ATLAS laser of our institute (Baumhacker *et al.*, 2002) are focused with an off-axis parabola to a spot 10 μm in diameter. The pulses had an energy of up to 600 mJ and a duration of 150 fs. The maximum intensities obtained were in the range of 10^{19} W/cm^2. Aluminum and copper foils with thicknesses ranging from 10 to 100 μm were used as the targets. The laser pulses were incident *p*-polarized at 45° to the target.

The Čerenkov medium used in the present study was a 60-μm thin foil of polypropylene. Due to its index of refraction of 1.48 and an insignificant fluorescence yield this material is well suited as a Čerenkov medium. In addition, a 60-μm path length of this low-*Z* substance has a negligible effect on the energy and direction of the electrons, allowing unaltered detection of the beams emerging from the primary target. The thin Čerenkov medium also allows imaging of the electron pattern with a relatively high resolution. With a thicker medium a higher emission is achieved, but at the expense of smearing the spatial pattern.

Visible Čerenkov radiation was collected behind the target by means of an *f*/2 objective and then recorded spatially resolved by an intensified gated CCD with gate duration of 5 ns. The CCD image thus gives a two-dimensional (2D) image of the cross section of the electron beam as it arrives at the rear side of the target. To block any light from the laser pulse and its harmonic, a 6-mm Schott BG18 filter and a 3-mm VG8 filter were inserted into the beam path.

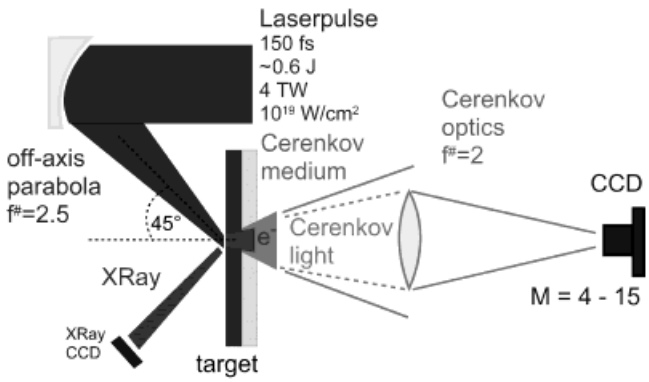

Fig. 1. Experimental arrangement used for X-ray and Čerenkov diagnostics of hot electrons.

https://doi.org/10.1017/S0263034604223163 Published online by Cambridge University Press

3. ELECTRONS PROPAGATING THROUGH FOILS

Spatial patterns of the radiation detected behind 100 μm of Al foil are shown in Figure 2. The figure gives two patterns obtained at intensities of 5×10^{18} and 10^{19} W/cm^2. Lineouts along the horizontal direction are also shown. It is striking that the higher intensity results in the appearance of two distinct maxima, whereas at the lower intensity only a dip in the pattern is discernible.

The interpretation of these results invokes two mechanisms generating the hot electrons, namely, resonance absorption and ponderomotive acceleration (Santala *et al*., 2000). The electron population due to resonance absorption propagates perpendicularly to the target surface, whereas the ponderomotively accelerated electrons are in line with the laser radiation. Semi-empirical scaling laws for the electron temperatures obtained with the two processes were derived, yielding (Beg *et al*., 1997)

$$kT_{\mathrm{ra}}\,(\mathrm{keV}) = 100\,(I_{17}\,\lambda^2)^{1/3} \tag{6}$$

for the electrons generated by resonance absorption and (Malka & Miquel, 1996)

$$kT_{\mathrm{pond}}\,(\mathrm{keV}) = 511\,[(1 + I_{17}\,\lambda^2/13.7)^{1/2} - 1] \tag{7}$$

for the electrons heated by ponderomotive acceleration. Here I_{17} is the intensity of the laser pulse in units of 10^{17} W/cm^2.

Using these scaling laws for the electron temperatures, one can evaluate the two peaks seen in the spatial Čerenkov pattern and derive the number of electrons in each electron population. For this evaluation it has to be taken into account that the original Boltzmann distribution of the electrons is altered by their propagation through the foil. We use the Bethe–Bloch formula (see, e.g., Birkhoff, 1960) to calculate the resulting electron energy distributions. Results of such calculations are shown in Figure 3, which also gives the limits of electron energies contributing to the Čerenkov radiation due to the values of β_{min} and β_{max} given above. The electron numbers and conversion efficiencies for the two

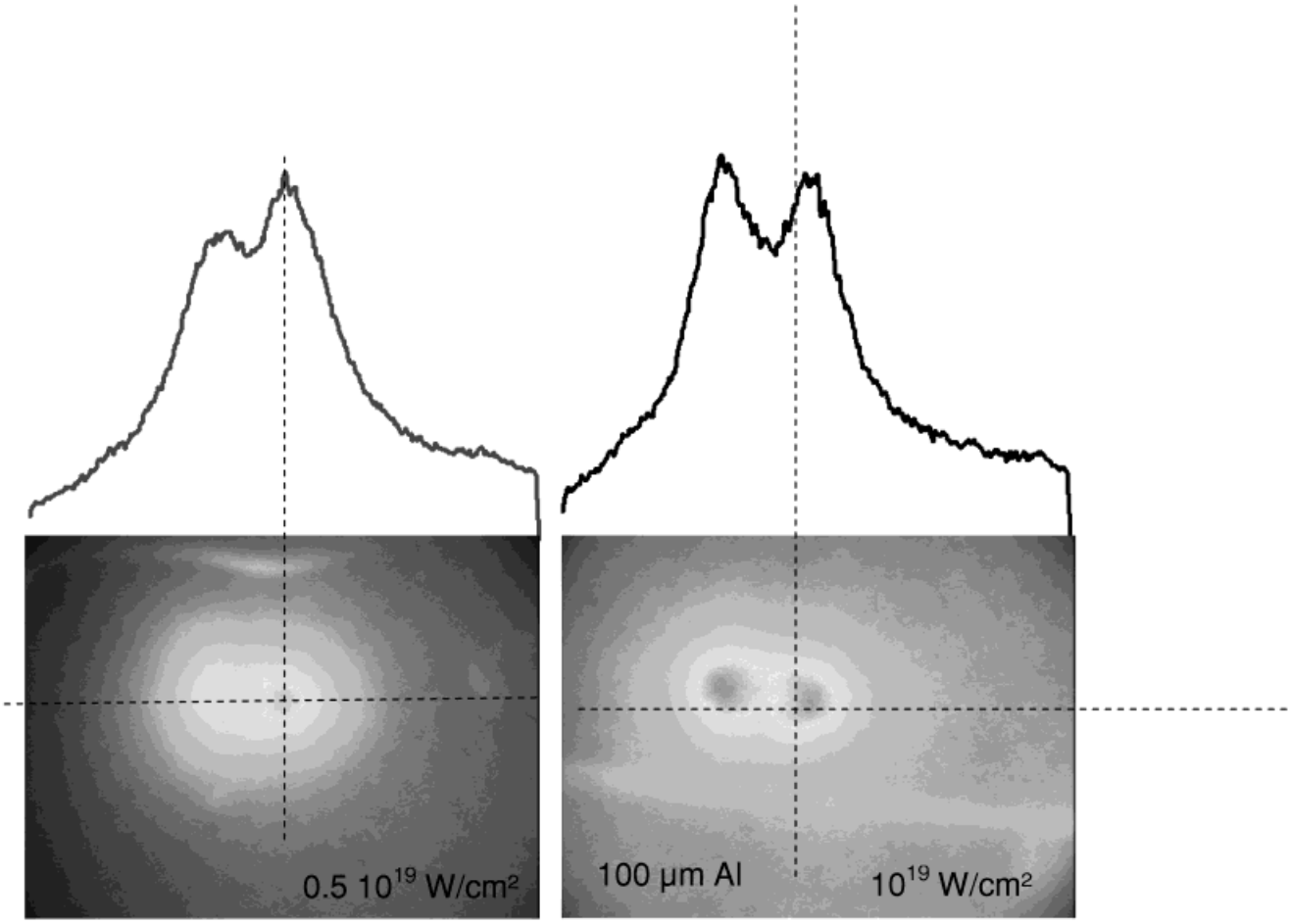

Fig. 2. Spatially resolved Čerenkov radiation behind 100-μm aluminum foil at intensities of 5×10^{18} and 10^{19} W/cm^2. The two peaks resulting from electrons propagating perpendicularly to the target surface and in line with the laser radiation are clearly visible. Lineouts shown are along dashed lines.

https://doi.org/10.1017/S0263034604223163 Published online by Cambridge University Press

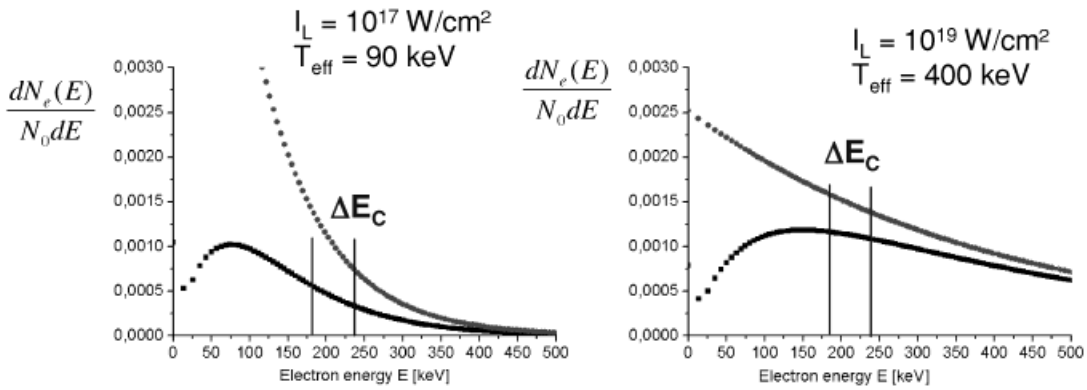

Fig. 3. Electron energy distributions behind 100-μm Al foil, calculated by means of the Bethe–Bloch formula. Input energies are Boltzmann distributions with temperatures given by Eq. (4) (perpendicular electrons). Limits of electron energies contributing to the detected Čerenkov radiation due to β_{min} and β_{max} as defined in the introduction are also shown.

populations obtained in this way are given in Figure 4. It is seen that the efficiencies in transferring laser energy into hot-electron energy due to resonance absorption and ponderomotive acceleration are quite different and depend strongly on the intensity of the radiation. The data show that the electron numbers detected by Čerenkov radiation are not much different for the two populations and that the higher efficiency into ponderomotively accelerated electrons is mainly due to the higher temperature generated by this mechanism.

4. ELECTRONS CROSSING VACUUM GAPS

The physics of electrons crossing thin vacuum gaps has important implications relating to X-ray irradiation experiments and ion acceleration. However, detailed studies of the transition of ultrashort high-current electron beams from the conductor into a vacuum are still lacking. Straightforward application of the Poisson equation predicts that large electrostatic fields are generated behind the target, slowing down the electrons or entirely preventing their propagation. The question to be answered is how close can one approach the target generating the radiation (henceforth called primary target) and still separate the effects of the X rays from those of the electrons.

The experiments and the theory presented in this article help to answer the above question. The method of investigation is to record the emission of an X-ray "fluor" (the secondary target) in immediate contact with the primary target and compare it with the emission when the fluor is placed at a distance behind it.

The targets used in these experiments are shown in Figure 5. A 10-μm copper foil is the primary target. The secondary target consists either of a 125-μm-thick plate of

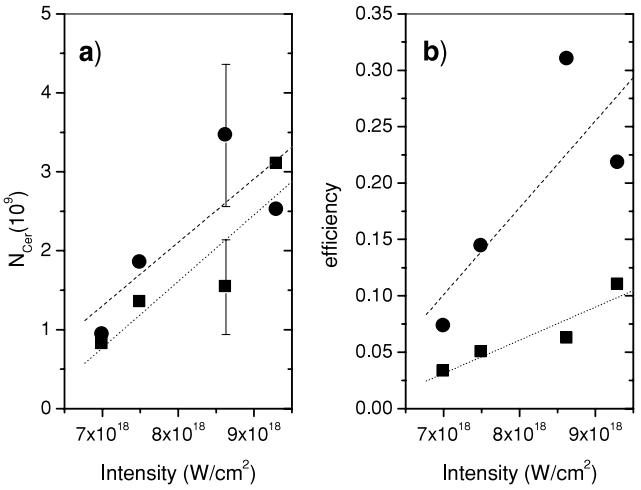

Fig. 4. a: Numbers of electrons detected by Čerenkov radiation as a function of intensity. b: Conversion efficiencies into hot electrons derived from these data. Squares: electrons perpendicular to the target surface (resonance absorption); circles: electrons in line with the laser (ponderomotive acceleration). Dashed and dotted lines display linear fits to the two sets of data.

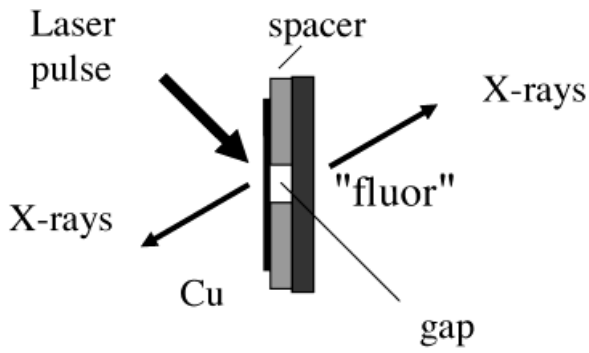

Fig. 5. Targets used for demonstrating the effect of self-fields of the electrons for preventing them from crossing narrow vacuum gaps. The primary target consists of a 10-μm copper foil. A spacer between primary and secondary targets generates gaps of different widths. The secondary targets ("fluors") consist of a 10-μm nickel foil or a 125-μm-thick molybdenum plate. For the experiments with Ni as a fluor, the X rays were detected behind, and for Mo fluor in front of the target.

https://doi.org/10.1017/S0263034604223163 Published online by Cambridge University Press

molybdenum or of 10-μm nickel foil. Gaps of 50 μm up to 500 μm were realized by means of a stainless-steel spacer between the primary and secondary targets. Taking advantage of the fact that the 17.4-keV Mo $K\alpha$ radiation is well transmitted through the 10-μm Cu primary target, the molybdenum experiments used the CCD placed in front of the target. The 20-keV K-edge of Mo is significantly above the photon energy of the copper K-shell lines and thus the amount of photopumping is expected to be small. For the experiments with nickel the CCD was placed behind the target and the X rays were observed in transmission. Again, photopumping is small, because the photon energy of Cu $K\alpha$ radiation is below the nickel K-edge.

The X rays generated by the electrons were detected by means of a backside-illuminated, thinned X-ray CCD in the single-photon mode. In this mode the generated charge is proportional to the energy of the photon and can thus be used to roughly disperse the detected radiation. The spectral resolution is improved by applying numerical event recognition techniques, which discriminate against so-called multipixel events in which the generated charge is distributed among many pixels (Owens *et al*., 1994).

The Mo $K\alpha$ photon yields for the two gap widths relative to the yields for no gap are shown in Figure 6. The strong drop in photon yield already at the smallest gap width of 50 μm is evident. With increasing gap width the photon yield is further reduced but at a lesser rate. Figure 6 also shows a theoretical curve obtained by a semi-analytical theory that combines the effect of the self-fields (Fill, 2001*a*) with Monte Carlo simulations of electron propagation through solid material. The self-fields induce a cutoff energy of the electrons that is the higher the larger the distance behind the target. Electrons with an initial energy below the cutoff energy are pulled back to the target.

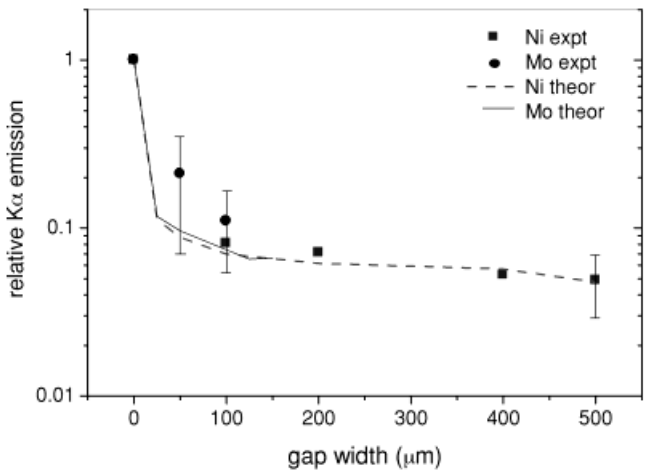

Fig. 6. Mo and Ni $K\alpha$ photon yield for gap widths ranging from 50 to 500 μm relative to the yield with no gap (fluor in immediate contact with primary target). The strong reduction in X-ray yield caused by a gap is evident. Theoretical curves obtained by an analytical theory are also displayed in the diagram.

For an infinitely short electron pulse in one dimension the cutoff energy can be calculated in the following way. Consider a one-dimensional electron beam with an areal density N_a entering a vacuum from a metallic solid. At a distance x from the solid a fraction of ξ of the electrons has travelled beyond that distance. The quantity ξ can be considered as a Lagrangian coordinate of the electrons. Straightforward integration of the Poisson equation yields the field experienced by electrons with the Lagrangian coordinate ξ as given by $E(\xi) = 4\pi e\xi N_a$ and thus the electrons experience a decelerating force given by $-eE(\xi)$. Equating the initial electron energy U to the work done on these electrons by the decelerating force one obtains the equation

$$U(\xi) = 4\pi e^2 \xi N_a x, \tag{8}$$

where x is the distance at which electrons with initial energy $U(\xi)$ are stopped. The Lagrangian coordinate $\xi(U)$ is calculated by integrating the electron energy distribution $f(U)dU$ from U to infinity and $U(\xi)$ is just its inverse. Solution of the transcendental Eq. (8) yields the cutoff energy $U(\xi)$ at a distance x from the solid. We note that with an exponential electron energy distribution, Eq. (8) becomes relatively simple, because $U(\xi)$ and its inverse $\xi(U)$ can then be expressed as analytical functions. This may work for an ultrathin foil. However, for 10 μm of copper the Monte Carlo simulations show that the electron distribution behind the primary target is considerably altered, reflecting the fact that fewer electrons with a low energy are transmitted. The theoretical curve is obtained by running the Monte Carlo code (Seltzer, 1991) with the respective cutoff energy. Two electron populations (resonance absorption and ponderomotively scattered electrons) are separately taken into account. A more detailed account of the theory is left to a further publication.

The simulation results agree reasonably well with the experimental data, the latter consistently exhibiting somewhat higher values. This may be explained by the fact that the electron energy distribution is shifted to lower energies upon propagation, and, owing to the higher cross section for K-hole generation at lower energies, more X rays are generated.

This study shows that self-fields generated by the electrons are indeed quite effective in stopping the propagation of a large fraction of them. However, electrons above the cutoff energy are still able to cross relatively large distances.

5. FUTURE INVESTIGATIONS

The method of Čerenkov diagnostics allows a number of further investigations on hot electrons to be made. The first of these relates to the spectrum of the Čerenkov radiation. The classical theory predicts a smooth spectrum exhibiting a monotonic rise of the emission at shorter wavelengths (see Eq. (3)). However, the ponderomotively scattered electrons should exhibit a component oscillating at the second harmonic of the laser frequency. This effect has already been

https://doi.org/10.1017/S0263034604223163 Published online by Cambridge University Press

observed using optical transition radiation (Baton *et al*., 2003). However, the second-harmonic component should be absent in the population generated by resonance absorption, and thus a spatially resolved spectrum of the Čerenkov radiation should reflect this feature in the two mechanisms generating the hot electrons.

A further interesting aspect to be investigated by Čerenkov diagnostics is the filamentation of the generated electron beams. The Weibel instability (Weibel, 1959) results in the generation of small current filaments with a diameter given approximately by the skin depth c/ω_p, where ω_p is the plasma frequency at the electron density of the solid (Lee & Lampe, 1973; Honda *et al*., 2000). This aspect is essential for relativistic electron transport in fast ignition of targets for inertial confinement fusion (Honda *et al*., 2000). The small skin depth leads to submicron diameters of the filaments in normal solids. However, using a low-density target material might significantly increase the diameter of the filaments and allow their detection by optical imaging.

A final example of using Čerenkov radiation for determining electron beam parameters relates to the time duration of the electron pulse. Theory shows that the emission of Čerenkov radiation is an infinitely short process. In a practical experiment the temporal resolution is limited by the dispersion of the medium, which results in different propagation velocities of the generated photons and thus spreads the emitted light flash. By observing only a limited spectral region of the radiation this effect is minimized and the duration of the Čerenkov radiation pulse should reflect the duration of the electron pulse. An experiment making use of the optical Kerr effect (Albrecht *et al*., 1992) could establish a cross-correlation between the laser pulse and the Čerenkov pulse and clarify if the generated electron pulse is as short as the laser pulse.

Measuring the electron pulse duration is a way to determine the duration of X-ray pulses generated by the electrons. Ultrashort hard X-ray pulses are essential in time-resolved X-ray diffraction experiments (Rose-Petruck *et al*., 1999; Rousse *et al*., 2001; Sokolowski-Tinten *et al*., 2003), for testing of optics for fourth-generation light sources, and for pumping of inner-shell X-ray lasers (Pretzler *et al*., 2001).

ACKNOWLEDGMENTS

A. Böswald and H. Haas are thanked for ensuring reliable operation of the ATLAS laser facility. We are grateful to W. Fölsner for fabricating the targets. This work was supported in part by the Commission of the Euratom/Max-Planck-Institut für Plasmaphysik Association.

REFERENCES

Albrecht, H.-S., Heist, P., Kleinschmidt, J., van Lap, D. & Schröder, T. (1992). Measurement of ultraviolet femtosecond pulses using the optical Kerr effect. *Appl. Phys. B* **55**, 362–364.

Batani, D., Giugliano, F., Hall, T. & Koenig, M. (2001). Interferometric measurement of preheating in laser shocks. *Phys. Rev. E* **64**, 047401–047405.

Baton, S.D., Santos, J.J., Amiranoff, F., Popescu, H., Gremillet, L., Koenig, M., Martinolli, E., Guilbaud, O., Rousseaus, C., Rabec Le Gloahec, M., Hall, T., Batani, D., Perelli, E., Scianitti, F. & Cowan, T. (2003). Evidence of ultrashort electron bunches in laser-plasma interactions at relativistic intensities. *Phys. Rev. Lett.* **91**, 105001–105005.

Baumhacker, H., Böswald, A., Haas, H., Witte, K.J., Andiel, U., Bayer, J., Dong, X., Dreher, M., Eidmann, K., Fischer, M., Hegelich, M., Kaluza, M., Karsch, S., Keller, G., Pretzler, G., Stehbeck, H. & Tsakiris, G. (2002). Advanced Titanium Sapphire Laser ATLAS, Report: Max-Planck-Institut für Quantenoptik.

Beg, F.N., Bell, A.R., Dangor, A.E., Danson, C.N., Fews, A.P., Glinsky, M.E., Hammel, M.E., Lee, P., Norreys, P.A. & Tatarakis, M. (1997). A study of picosecond laser-solid interactions up to 10^{19} W/cm^2. *Phys. Plasmas* **4**, 447–457.

Birkhoff, R.D. (1960). *The passage of fast electrons through matter*. Berlin: Springer.

Borghesi, M., Mackinnon, A.J., Bell, A.R., Malka, G., Vichers, C., Willi, O., Davies, J.R., Pukhov, A. & Meyer-ter-Vehn, J. (1999). Observation of collimated ionization channels in aluminum-coated glass targets irradiated by ultraintense laser pulses. *Phys. Rev. Lett.* **83**, 4309–4312.

Brandl, F., Pretzler, G., Habs, D. & Fill, E. (2003). Cerenkov radiation diagnostics of hot electrons generated by fs-laser interaction with solid targets. *Europhys. Lett.* **61**, 632–638.

Davies, J.R., Bell, A.R. & Tatarakis, M. (1999). Magnetic focusing and trapping of high-intensity laser-generated fast electrons at the rear of solid targets. *Phys. Rev. E* **59**, 6032–6036.

Eder, D.C., Pretzler, G., Fill, E., Eidmann, K. & Saemann, A. (2000). Spatial characteristics of K-alpha radiation from weakly relativistic laser plasmas. *Appy Phys. B* **70**, 211–217.

Feurer, T., Morak, A., Uschmann, I., Ziener, C., Schwoerer, H., Förster, E. & Sauerbrey, R. (2001). An incoherent sub-picosecond X-ray source for time-resolved X-ray-diffraction experiments. *Appl. Phys. B* **72**, 15–20.

Fill, E. (2001*a*). Analytical theory of pulsed relativistic electrons beams entering a vacuum. *Phys. Plasmas* **8**, 4613–4617.

Fill, E. (2001*b*). Relativistic electron beams in conducting solids and dense plasmas: Approximate analytical theory. *Phys. Plasmas* **8**, 1441–1444.

Forslund, D.W., Kindel, J.M. & Lee, K. (1977). Theory of Hot-Electron Spectra at High Laser Intensity. *Phys Ref. Lett.* **39**, 284–287.

Gibbon, P. & Förster, E. (1996). Short-pulse laser-plasma interactions. *Plasma Phys. Control. Fusion* **38**, 769–793.

Gremillet, L., Amiranoff, F., Baton, S.D., Gauthier, J.-C., Koenig, M., Martinolli, E., Pisani, F., Bonnaud, G., Lebourg, C., Rousseaux, C., Toupin, C., Antonicci, A., Batani, D., Bernardinello, A., Hall, T., Scott, D., Norreys, P., Bandulet, H. & Pepin, H. (1999). Time-resolved observation of ultrahigh intensity laser-produced electron jets propagating through transparent solid targets. *Phys. Rev. Lett.* **83**, 5015–5018.

Hegelich, M., Karsch, S., Pretzler, G., Habs, D., Witte, K., Guenther, W., Allen, M., Blazevic, A., Fuchs, J., Gauthier, J.C., Geissel, M., Audebert, P., Cowan, T. & Roth, M.

(2002). MeV ion jets from short-pulse laser interaction with thin foils. *Phys. Rev. Lett.* **89**, 085002–085005.

Honda, M., Meyer-ter-Vehn, J. & Pukhov, A. (2000). Two-dimensional particle-in-cell simulation for magnetized transport of ultra-high relativistic currents in plasma. *Phys. Plasmas* **7**, 1302–1308. Jelley, JV. (1958). *Cerenkov Radiation and its Applications*. London, Pergamon Press.

Jelley, JV. (1958). *Cerenkov Radiation and its Applications.* London: Pergamon Press.

Lee, R. & Lampe, M. (1973). Electromagnetic instabilities, filamentation, and focusing of relativistic electron beams. *Phys. Rev. Lett.* **31**, 1390–1393.

Malka, G. & Miquel, J.L. (1996). Experimental confirmation of ponderomotive-force electrons produced by an ultrarelativistic laser pulse on a solid target. *Phys. Rev. Lett.* **77**, 75–78.

Owens, A., Mineo, T., McCarthy, K.J. & Wells, A. (1994). Event recognition in X-ray CCDs. *Nucl. Instrum. Methods Phys. Res. A* **346**, 353–365.

Pretzler, G., Schlegel, T. & Fill, E. (2001). Characterization of electron beam propagation through foils by innershell X-ray spectroscopy. *Laser and Particle Beams* **19**, 91–97.

Pretzler, G., Schleges, T., Fill, E. & Eder, D.C. (2000). Hot-electron generation in copper and photopumping of cobalt. *Phys. Rev. E* **62**, 5618–5623.

Rose-Petruck, C., Jimenez, R., Guo, T., Cavalleri, A., Siders, C.W., Raksi, F., Squier, J.A., Walker, B.C., Wilson, K.R. & Barty, C.P.J. (1999). Picosecond-milliangström lattice dynamics measured by ultrafast X-ray diffraction. *Nature* **398**, 310–312.

Rousse, A., Rischel, G., Fourmaux, S., Uschmann, I., Sebban, S., Grillon, G., Balcou, P., Förster, E., Geindre, J.P., Audebert, P., Gauthier, J.C. & Hulin, D. (2001). Non-thermal melting in semiconductors measured at femtosecond resolution. *Nature* **410**, 65–68.

Santala, M.I.K., Zepf, M., Watts, I., Beg, F.N., Clark, E., Tatarakis, M., Krushelnik, K., Dangor, A.E., McCanny, T., Spencer, I., Singhal, R.P., Ledingham, K.W.D., Wilks, S.C., Machacek, A.C., Wark, J.S., Allott, R., Clarke, R.J. & Norreys, P.A. (2000). Effect of the plasma density scale length on the direction of fast electrons in relativistic laser-solid interactions. *Phys. Rev. Lett.* **84**, 1459–1462.

Santos, J.J., Amiranoff, F., Baton, S.D., Gremillet, L., Koenig, M., Martinolli, E., Rabec Le Gloahec, M., Rousseaux, C., Batani, D., Bernardinello, A., Greison, G. & Hall, T. (2002). Fast Electron Transport in Ultraintense Laser Pulse Interaction with Solid Targets by Rear-Side Self-Radiation Diagnostice. *Phys. Rev. Lett.* **89**, 025001–025004.

Seltzer, S.M. (1991). Electron-Photon Monte Carlo Calculations: The ETRAN Code. *Appl. Radiat. Isot.* **42**, 917–941.

Snavely, R.A., Key, M.H., Hatchett, S.P., Cowan, T.E., Roth, M., Phillips, T.W., Stoyer, M.A., Henry, E.A., Sangster, T.C., Singh, M.S., Silks, S.C., MacKinnon, A., Johnson, J., Perry, M.D. & Campbell, E.M. (2000). Intense high-energy proton beams from Petawatt-Laser irradiation of solids. *Phys. Rev. Lett.* **85**, 2945–2948.

Sokolowski-Tinten, K., Blome, C., Blums, J., Cavalleri, A., Dietrich, C., Tarasevitch, A., Uschmann, I., Förster, E., Kammler, M., Horn-von-Hoegen, M. & von der Linde, D. (2003). Femtosecond X-ray measurement of coherent lattice vibrations near the Lindemann stability limit. *Nature* **422**, 287–289.

Tabak, M., Hammer, J., Glinsky, M.E., Kruer, W.L., Wilks, S.C., Woodworth, J., Campbell, E.M. & Perry, M.D. (1994). Ignition and high gain with ultrapowerful lasers. *Phys. Plasmas* **1**, 1626–1634.

Weible, E.S. (1959). Spontaneously growing transverse waves in a plasma due to an anisotropic velocity distribution. *Phys. Rev. Lett.* **2**, 83–85.

Wilks, S.C., Kruer, W.L., Tabak, M. & Langdon, A.B. (1992). Absorption of ultra-intense laser pulses. *Phys. Rev. Lett.* **69**, 1383–1386.

Wilks, S.C., Langdon, A.B., Cowan, T.E., Roth, M., Singh, M., Hatchett, S., Key, M.H., Pennington, S.D., MacKinnon, A. & Snavely, R.A. (2001). Energetic proton generation in ultra-intense laser-solid interactions. *Phys. Plasmas* **8**, 542–549.

https://doi.org/10.1017/S0263034604223163 Published online by Cambridge University Press